

Article

Manufacturing Elements with Small Cross-Sections of 17-4 PH Steel (1.4542) with the Application of the DMLS Additive Manufacturing Method

Grzegorz Budzik ¹, Łukasz Przeszlowski ^{1,*}, Tomasz Dziubek ¹, Małgorzata Gontarz ¹, Mariusz Dębski ¹ and Emil Smyk ²

¹ Department of Mechanical Engineering, Rzeszow University of Technology, al. Powstańców Warszawy 12, 35-959 Rzeszow, Poland; gbudzik@prz.edu.pl (G.B.); tdziubek@prz.edu.pl (T.D.); m.gontarz@prz.edu.pl (M.G.); m.debski@prz.edu.pl (M.D.)

² Faculty of Mechanical Engineering, UTP University of Science and Technology in Bydgoszcz, al. prof. S.Kaliskiego, 85-796 Bydgoszcz, Poland; emil.smyk@utp.edu.pl

* Correspondence: lprzeszl@prz.edu.pl

Abstract: The application of direct metal laser sintering renders it possible to manufacture models with complex geometries. However, there are certain limits to the application of this method connected with manufacturing thin-walled cuboidal elements, as well as cylinders and holes with small diameters. The principal objective of the research was to determine the accuracy of manufacturing geometries with small cross-sections and the possibility of application in heat exchangers that are radiators with radially arranged ribs. To that end, four specimens were designed and manufactured; their geometries of representations assumed for the purpose of research (analysis) changed dimensions within the following scope: 10–0.1 mm. The specimens to be applied in the research were manufactured with 17-4 PH stainless steel (1.4542) with the application of 3D-DMLS printing and an EOS M270 printer. The measurement of accuracy was performed with the application of an optical stereomicroscope (KERN OZL-466). In addition to that, research into the chemical composition of the material, as well as the size of spherical agglomerates, was conducted with the application of a scanning electron microscope. The analysis of the chemical composition was conducted as well (after the sintering process). The analysis of the results based on the values received by means of measurements of the manufactured geometries was divided into three parts. Based on this, it is possible to conclude that the representation of models manufactured with the application of DMLS was comparable with the assumptions, and that the deviations between a nominal dimension and that received in the course of the research were within the following scope: 0–0.1 mm. At the final stage of research and based on the received results, two heat exchangers were manufactured.

Keywords: additive manufacturing; DMLS; radiator; quality control; elements with small cross-sections



Citation: Budzik, G.; Przeszlowski, L.; Dziubek, T.; Gontarz, M.; Dębski, M.; Smyk, E. Manufacturing Elements with Small Cross-Sections of 17-4 PH Steel (1.4542) with the Application of the DMLS Additive Manufacturing Method. *Materials* **2021**, *14*, 3256. <https://doi.org/10.3390/ma14123256>

Academic Editor:
Federico Mazzucato

Received: 29 April 2021
Accepted: 10 June 2021
Published: 12 June 2021

Publisher's Note: MDPI stays neutral with regard to jurisdictional claims in published maps and institutional affiliations.



Copyright: © 2021 by the authors. Licensee MDPI, Basel, Switzerland. This article is an open access article distributed under the terms and conditions of the Creative Commons Attribution (CC BY) license (<https://creativecommons.org/licenses/by/4.0/>).

1. Introduction

Throughout recent years, it has been possible to observe a significant development in rapid prototyping methods, which is contributed to by an ever-greater interest of numerous industries such as the aviation industry [1–10]. In practice, DMLS (direct metal laser sintering) is an alternative to models manufactured with the application of casting processes. It consists of sandwich direct metal laser sintering with the application of a fiber ytterbium laser [11,12]. The material is taken from a dispenser and afterward placed in layers with the application of a drift fender in the working space (height of a layer is dependent upon the kind of material in a dispenser; possible range: 10–80 μm). Parts are manufactured directly based on a three-dimensional computer aided design (3D CAD) model (after appropriate data processing—recording in the “stl” format), owing to which

it is possible to shorten the time required to manufacture single items or short lots. An additional advantage is that it renders it possible to avoid so-called indirect modeling, and, consequently, to reduce the inaccuracy of dimensions. This method renders it possible to manufacture models with a complex geometry, frequently impossible to manufacture with the application of conventional manufacturing methods [13,14]. Unfortunately, however, limits to the application of this method connected with manufacturing thin-walled cuboidal elements, and also cylinders and holes with a small diameter, ought to be taken under consideration. It is also a very important aspect to manufacture such geometries with appropriate accuracy, and also to ensure allowances for further post-processing [15,16].

The objective of this article was to present the possibilities of manufacturing geometries with small cross-sections of 17-4 PH stainless steel (1.4542) with the application of 3D-DMLS printing and an EOS M270 printer. In the literature of the subject, it is possible to find information relevant to designing selected geometries for the needs of additive manufacturing with the application of a selected method of it. In the case of cuboidal structures, it is most frequently the minimum thickness of an unsupported wall that is referred to; it amounts to 0.4 mm (Figure 1a). The situation is similar in the case of unsupported cylindrical structures, yet, as far as they are concerned, the diameter amounts to 0.1 mm (Figure 1b) [17–21].

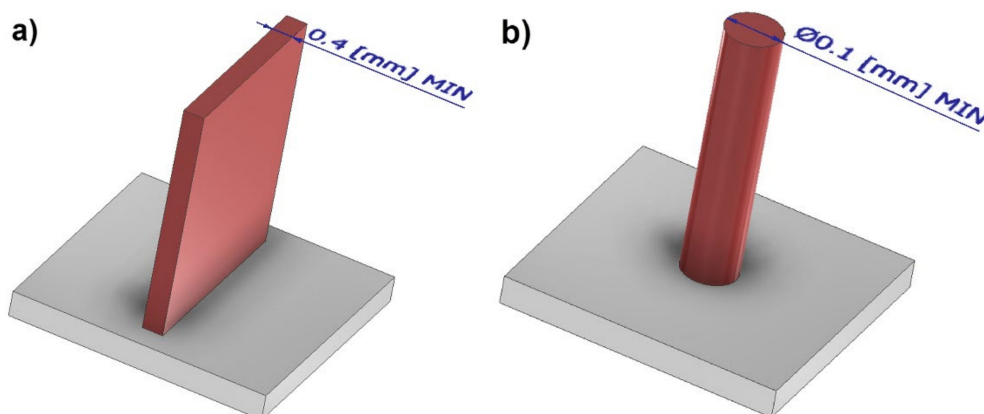


Figure 1. Elements with small cross-sections: (a) cuboidal; (b) cylindrical.

The research was conducted to manufacture heat exchangers radiators with radially arranged ribs with the application of 3D printing. The radiators were designed in two variants presented in Figures 2 and 3. The principal assumptions in the course of designing a radiator were a heat exchange surface exceeding 0.1 m², the number of ribs, their radial arrangement, and limits connected with the size of the working space of an EOS M270 printer [22].

In addition to that, in Figures 2 and 3, the location of the XY plane, as well as the direction of a drift fender movement (red arrow) in the working space of an additive device, is presented.

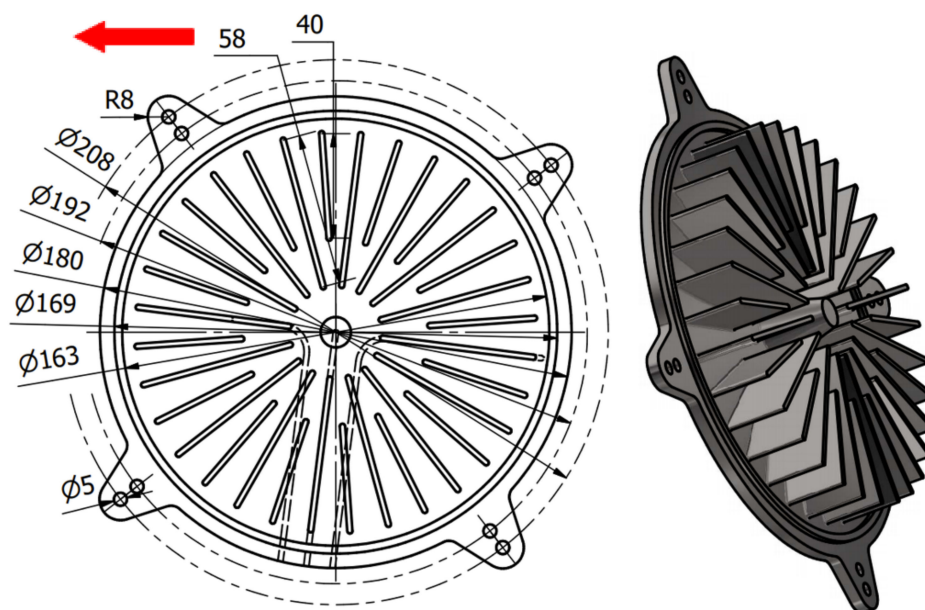


Figure 2. Illustrative drawing of radiator variant No. 1.

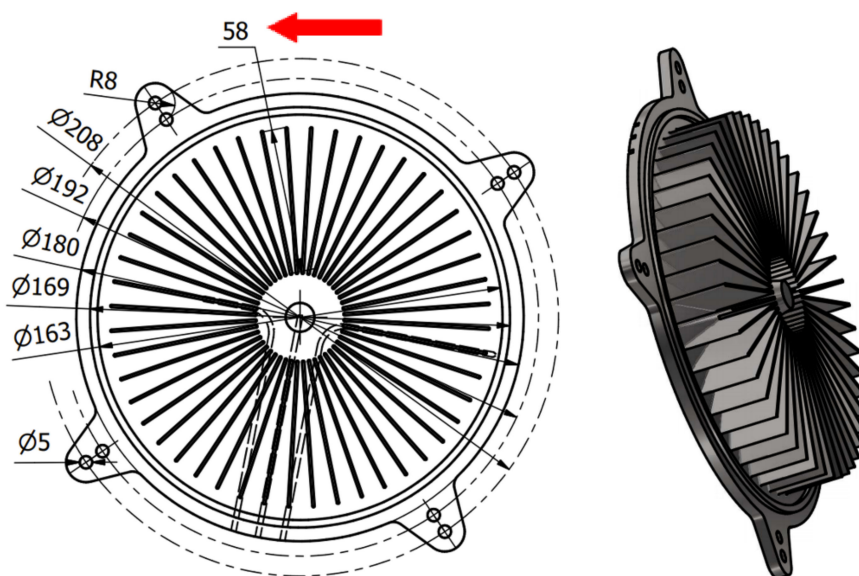


Figure 3. Illustrative drawing of radiator variant No. 2.

2. Materials and Methods

2.1. Materials

For manufacturing specimens with the application of DMLS, the 17-4 PH stainless steel (1.4542) of the EOS company (trade name: GP1) (EOS GMBH, Krailling, Germany) was applied as a powder in the form of spherical particles with a grain size between 20 and 80 μm . To verify the data provided by the producer and relevant to the chemical composition of a material (Table 2), as well as to the size of the spherical particles, a scanning electron microscope was applied to research the powder (Figure 4). In addition to that, the analysis of the chemical composition after the sintering process was conducted (Table 1). The area of the microanalysis of chemical composition SEM is presented in Figure 5. In Table 3, the selected mechanical properties of the 17-4 PH stainless steel, applied in the course of manufacturing the analyzed research models, are collated. The presented data are available on the website of the producer.

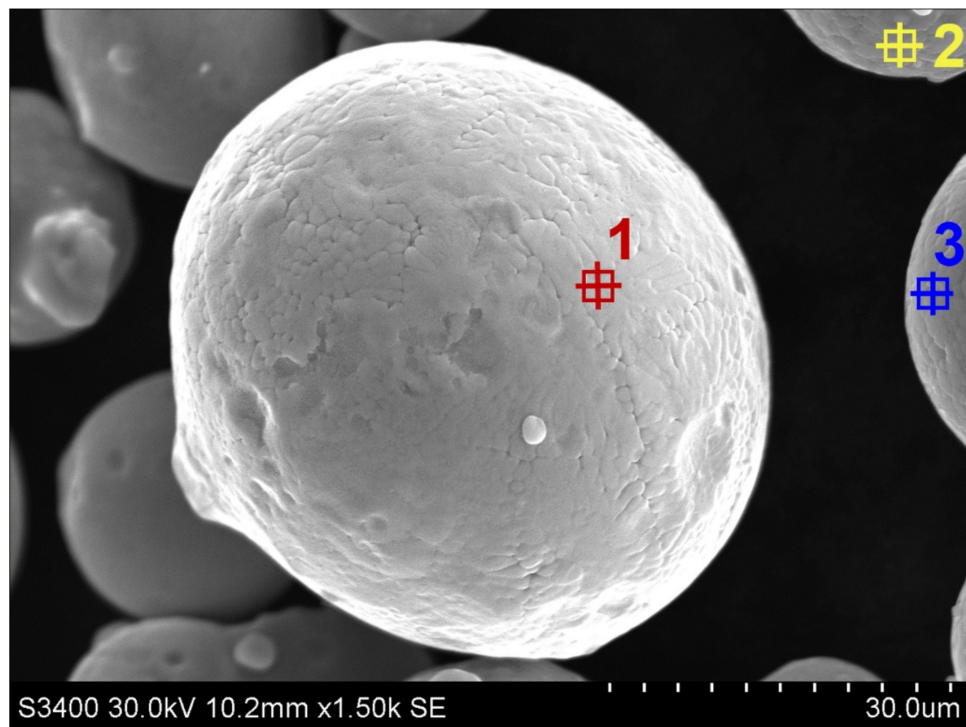


Figure 4. Example of 17-4 PH stainless-steel spherical particles (1,2,3- measurement points).

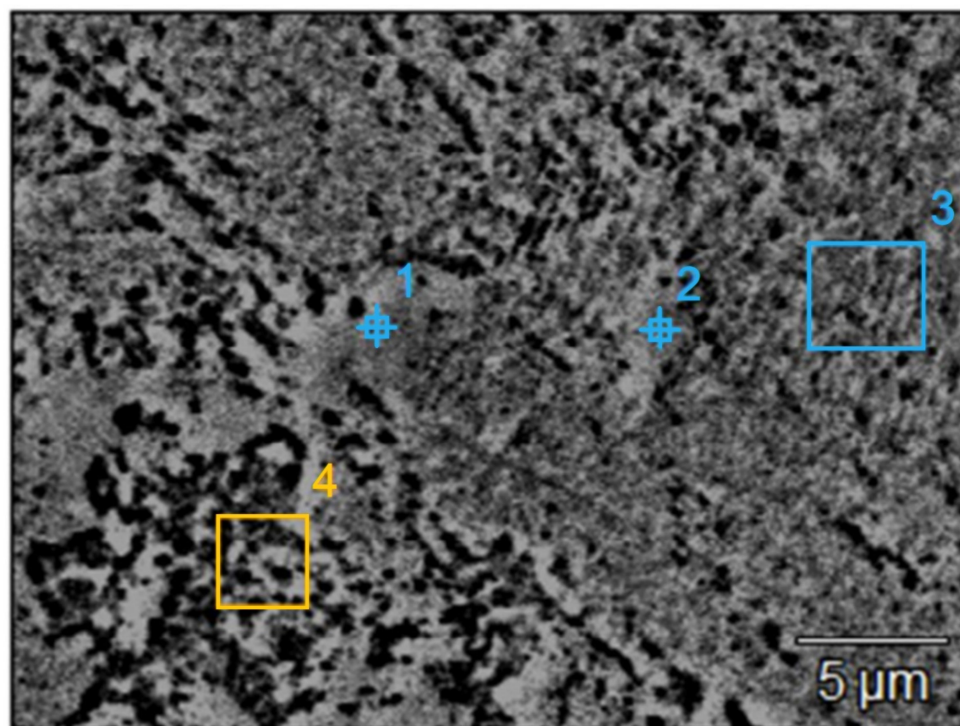


Figure 5. The area of microanalysis of the chemical composition of SEM sample after sintering (1,2- measurement points; 3,4- measurement areas).

Table 1. The chemical composition of DMLS sintered parts (areas are shown in Figure 5).

Area	Si-K (%)	Cr-K (%)	Mn-K (%)	Fe-K (%)	Ni-K (%)	Cu-K (%)	Nb-K (%)	Ta-L (%)
1	1.9	16.6	1.0	69.5	3.8	3.7	0.2	0.0
2	1.4	17.5	0.9	72.3	4.2	3.6	0.1	0.0
3	1.2	17.4	1.1	72.6	4.0	3.5	0.1	0.0
4	1.4	17.3	1.1	72.4	4.0	3.6	0.2	0.1

Table 2. The chemical composition of 17-4 PH steel (areas are shown in Figure 4).

Area	Si-K (%)	Cr-K (%)	Mn-K (%)	Fe-K (%)	Ni-K (%)	Cu-K (%)	Nb-K (%)	Ta-L (%)
1	4.3	16.9	0.9	70.8	4.0	3.0	0.0	0.0
2	2.1	17.1	1.0	72.1	4.0	3.4	0.3	0.0
3	1.3	18.2	1.1	70.1	4.3	4.2	0.6	0.1

Table 3. Selected material data of stainless steel 17-4 PH.

Alloy designation	17-4 (United States) 1.4542 (Europe) X5CrNiCuNb16-4 (Germany)
Geometric Data	
Minimum recommended layer thickness [μm]	20
Typical achievable part accuracy	a. $\pm 20 \div 50 \mu\text{m}$ (small parts) b. $\pm 0.2\%$ (large parts) ¹
Minimum wall thickness [mm]	0.3 \div 0.4
Surface roughness	a. $R_a: 2.5 \div 4.5 \mu\text{m}$, $R_y: 15 \div 40 \mu\text{m}$ (after shot-peening) b. $R_z \text{ do} < 0.5 \mu\text{m}$ (detail can be very finely polished) (after polishing)
Mechanical Properties of Parts	
Ultimate tensile strength [MPa]	a. min. 850, typical 930 ± 50 (XY); min. 850, typical 960 ± 50 (Z) ² b. typical 1100 (XY); typical 980 (Z) ³
Elongation at break [%]	a. min. 25, typical 31 ± 5 (XY); min. 25, typical 35 ± 5 (Z) ² b. typical 29 (XY); typical 31 (Z) ³
Modulus of elasticity (Young's modulus) [GPa]	a. 170 ± 30 ² b. typical 180 ³
Upper yield strength [MPa]	a. min. 595, typical 645 ± 50 (XY); min. 580, typical 630 ± 50 (Z) ² b. typical 634 (XY); typical 595 (Z) ³
Lower yield strength [MPa]	a. min. 530, typical 586 ± 50 (XY); min. 530, typical 570 ± 50 (Z) ² b. typical 590 (XY); typical 550 (Z) ³
Hardness	a. as built: ok. 230 ± 20 HV1, i.e., approx. 18.0 ± 1.6 HRC ok. 250 HV1 \div 400 HV1, i.e., approx. $22.2 \div 40.8$ HRC

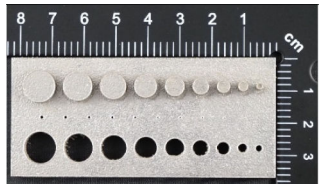
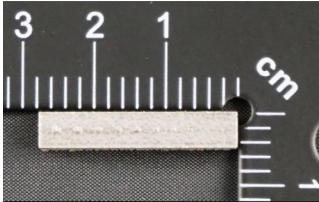
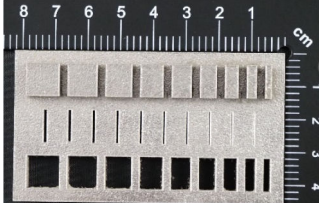
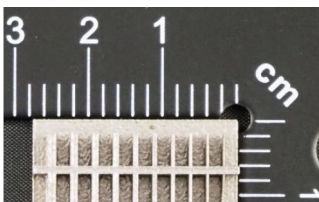
Comment: ¹—the accuracy can be improved by post-process stress-relieving for 1 h at 650 °C; ²—as manufactured; ³—stress relieved (1 h at 650 °C).

2.2. DMLS Part Manufacturing

Specimens to be applied in the research were manufactured of the powder of the high-chromium DMLS steel with the application of an EOSINT M270 printer (EOS GMBH, Krailling, Germany) and designed in the Autodesk Inventor Professional 2020 environment (Autodesk, Inc., Mill Valley, CA, USA), to be exported afterward to an STL surface format. The base size and the location of particular elements of the researched geometry were selected to render it possible to manufacture the details in question with the application of direct metal laser sintering [16,17,23]. For the purpose of analyzing the accuracy of the representation of the geometry of prototypes manufactured with the application of DMLS,

four research models (marked as presented in Table 4) were applied. The rationale behind the designed geometry of the specimen is the time required for printing. Manufacturing a single heat exchanger requires approximately 80 h, which, in the case of the conducted research, would result in a significantly extended manufacturing time and in an increased consumption of the material.

Table 4. Research models.

No.	Description	Mark	View
1.	base with cylindrical holes and cylinders with diameters from $\text{Ø}10$ to $\text{Ø}2$ mm and cylindrical holes with diameters from $\text{Ø}1$ to $\text{Ø}0.1$ mm	MB1	
2.	base with cylinders with diameters from $\text{Ø}1$ to $\text{Ø}0.1$ mm	MB2	
3.	base with cuboidal objects 10 to 2 mm wide and rectangular holes 10 to 2 mm wide and 1 to 0.1 mm wide	MB3	
4.	base with cuboidal objects 1 to 0.1 mm wide	MB4	

In Figure 6a–d, the dimensions of the specimen marked MB1 are presented. In the upper part of the specimen, there are cylinders with the following diameters: $\text{Ø}10$ – $\text{Ø}2$ mm, with a step of 1 mm (from the left—cross-section A–A—Figure 6b), and below, there are holes with the following diameters: $\text{Ø}1$ – $\text{Ø}0.1$ mm, with a step of 0.1 mm (from the left—cross-section B–B—Figure 6c). In turn, in the lower part of the object presented in cross-section C–C (Figure 6d), there are holes with the following diameters: $\text{Ø}10$ – $\text{Ø}2$ mm, with a step of $\text{Ø}1$ mm. In Figure 7a,b, cylinders with the following diameters: $\text{Ø}1$ – $\text{Ø}0.1$ mm, with a step of 0.1 mm, with the specimen marked MB2 from the left, are presented.

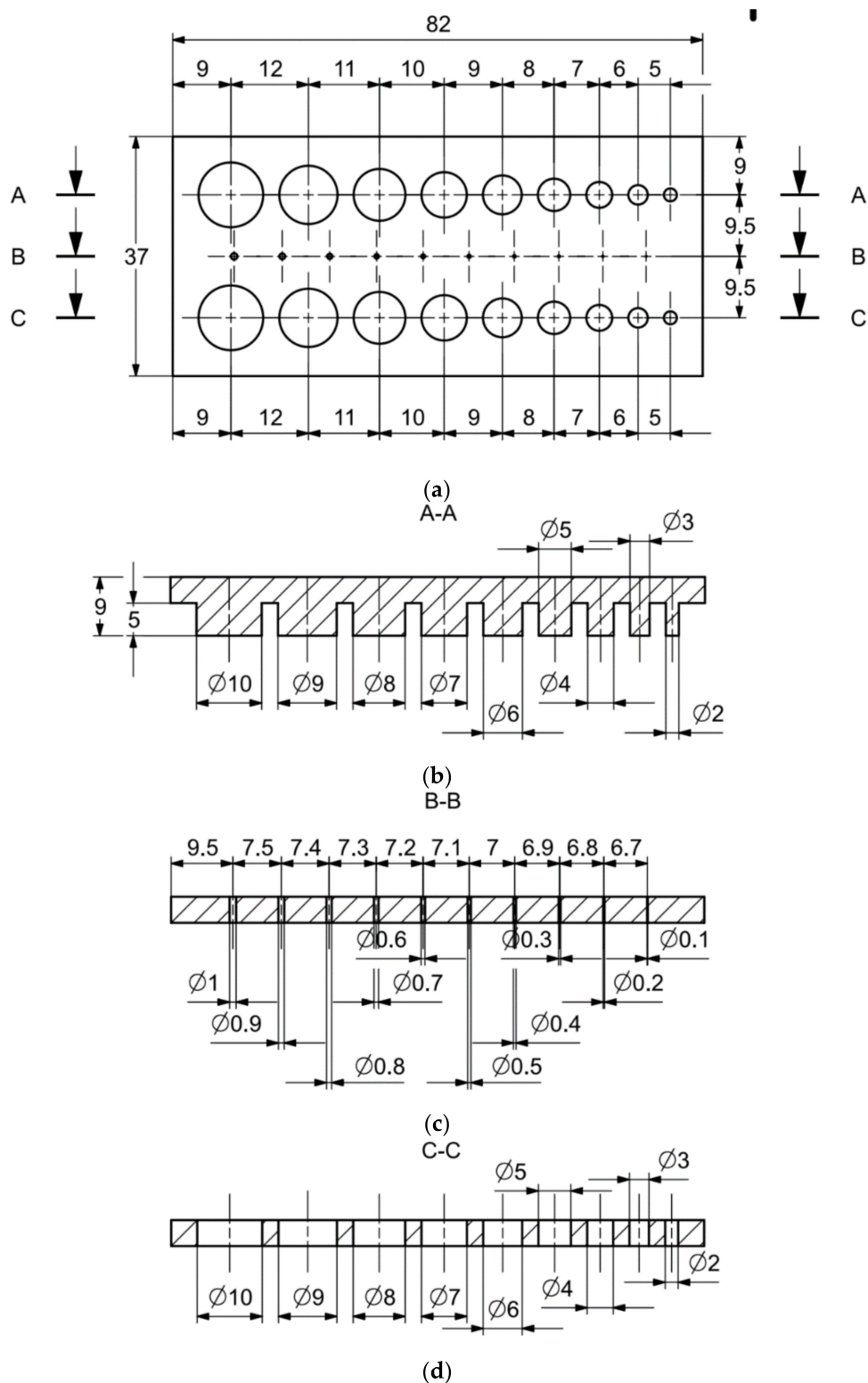


Figure 6. (a) The main view of the illustrative drawing of samples covered by the research is marked as MB1. (b) The A-A cross-section of cylinders $\text{Ø}10\text{--}\text{Ø}2$ mm based on Figure 6a of the main view of an illustrative drawing of samples covered by the research is marked as MB1. (c) The B-B cross-section of holes $\text{Ø}1\text{--}\text{Ø}0.1$ mm based on Figure 6a of the main view of an illustrative drawing of samples covered by the research is marked as MB1. (d) The C-C cross-section of holes $\text{Ø}10\text{--}\text{Ø}2$ mm based on Figure 6a of the main view illustrative drawing of samples covered by the research is marked as MB1.

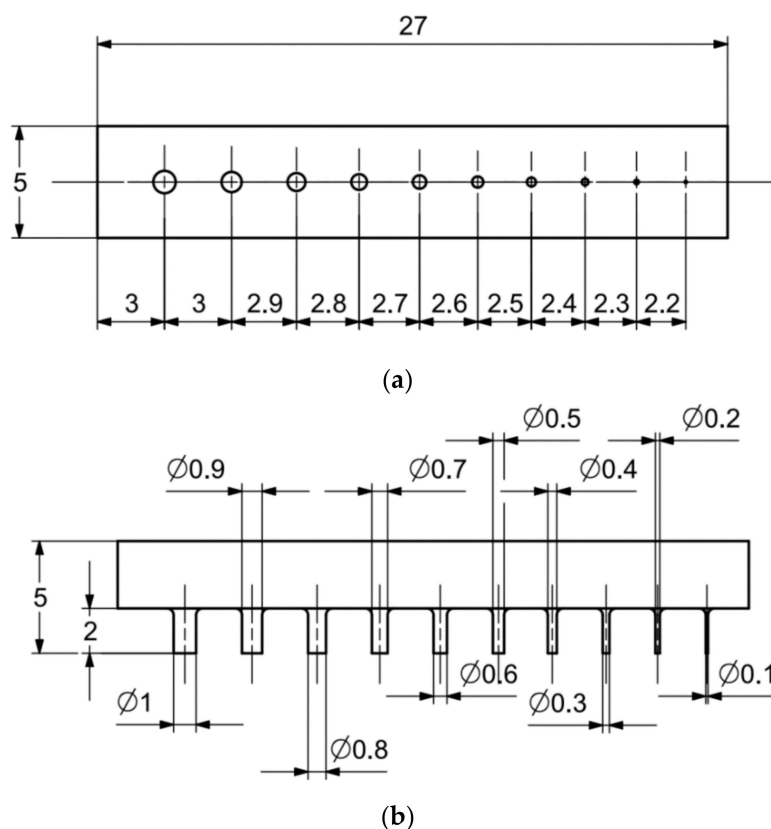


Figure 7. (a) The illustrative drawing of samples covered by the research is marked as MB2. (b) The top view of cylinders $\text{Ø}1\text{--}\text{Ø}0.1$ mm based on Figure 7a of the main view of an illustrative drawing of samples covered by the research is marked as MB2.

In the case of the research models marked MB3, as well as MB4, presented in Figures 8 and 9, it is solely the width of the geometry that is changed. In the upper part of the specimen marked MB3 (Figure 8a), from the left, there are cuboidal objects with the following widths: 10–2 mm (with a step of 1 mm—cross-section A-A—Figure 8b), and below them, there are holes with the following widths: 1–0.1 mm, with a step of 0.1 mm (cross-section B-B—Figure 8c), and, in the lowest part of the discussed element, there are holes with the following dimensions: 10–2 mm with a step of 1 mm (cross-section C-C—Figure 8d). In turn, in Figure 9a,b, there are cuboidal objects with the following widths (from the left): 1–0.1 mm (with a step of 0.1 mm).

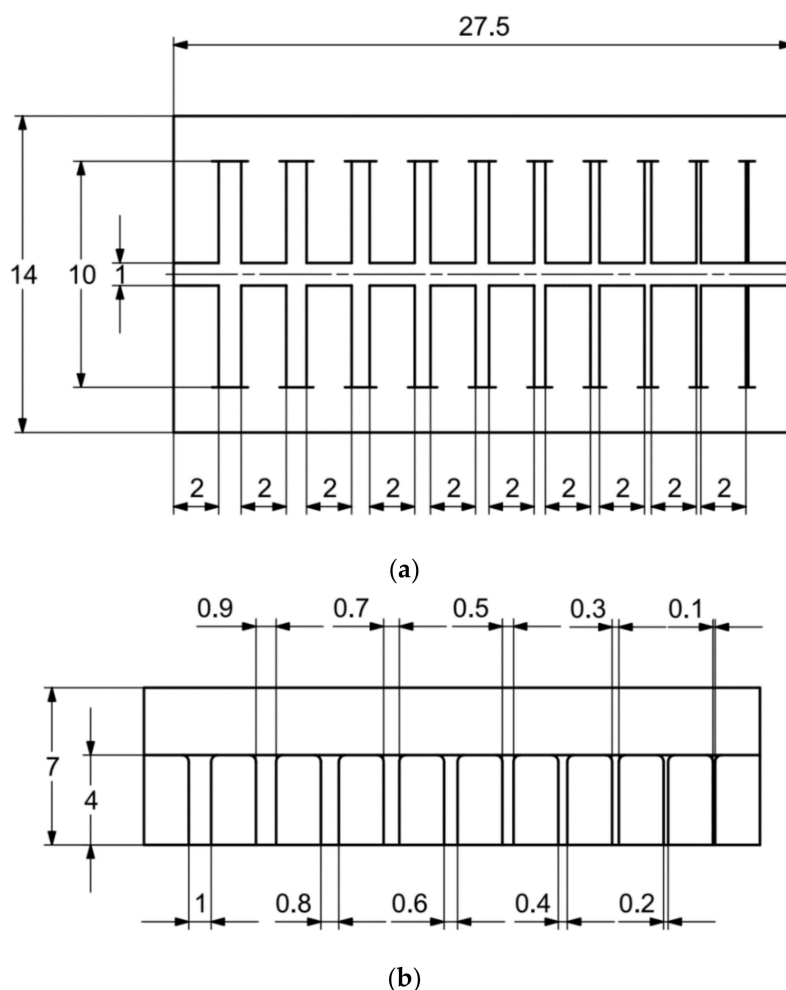


Figure 9. (a) The main view of the illustrative drawing of samples covered by the research is marked as MB4. (b) The top view of cuboidal objects 1–0.1 mm based on Figure 9a of the main view of an illustrative drawing of samples covered by the research is marked as MB4.

The models presented in Figures 6–9 were manufactured of the powder of the high-chromium GP1 steel (EN 1.4572, 17-4 PH) with the application of an EOS M270 printer. Prior to starting the printer, “stl” model files were read in the Magics program of the Materialise company. In this program, the best possible location of the details in the virtual working space of a prototyping device was determined, and the supporting structures were defined. After verifying the correctness of the model representations, the program was applied to generate an “sli” file, containing, among others, information on the layer height (20 μm) and the location of the models on the working plane of the prototyping device, and also a “cli” file, with information on the supporting structure. Afterward, the file with information on the support was exported to an “sli” file.

In the course of pre-processing, a printing device was prepared: a laser was heated up, material residues were removed, steel powder was prepared for printing, and the work table was leveled. Afterward, the “sli” files were transferred to a program dedicated to the manufacturing process on an EOS M270 printer. This program renders it possible to determine such parameters of sintering as laser rapidity in the course of contour sintering, and also fillings, the height of the sintered layer, or laser power in the course of scanning the appropriate areas. The basic parameters of sintering are presented in Table 5.

Table 5. Selected parameters of the sintering process in the DMLS method.

Type of Parameter	Mark	Unit	Value
Layer thickness	d	(mm)	0.2
Laser power during sintering	P_{laser}	(W)	180
First contour sintering speed	v_{K1}	(mm/s)	1200
Value of the first contour offset from the CAD model contour	BO_1	(mm)	0.06
First contour sintering width	SB_1	(mm)	0.09
Sintering speed of the initial or final layers inside the contour	v_H	(mm/s)	1200
Width of the inner layer melt with the contour of the initial and final layers	h_H	(mm)	0.1
Core sintering speed	v_K	(mm/s)	1250
Width of the inner layer melt input with the core layer contour	h_K	(mm)	0.08
Sintering speed of the second contour coinciding with the contour of the CAD model	v_{K2}	(mm/s)	2200
Value of the second contour offset from the CAD model contour	BO_2	(mm)	0.06
Second contour sintering width	SB_2	(mm)	0.08

At the further stage (post-processing), the received research models underwent initial purification and were also removed from the printer work table with the application of a hack-saw. Only the model-supporting structures were subjected to grinding.

2.3. Research Methodology Relevant to Geometrical Parameters

The measurements of elements were performed with the application of an optical stereomicroscope (KERN OZL-466, KERN & SOHN GMBH, Balingen, Germany), which was calibrated for every researched height. Every considered size was measured three times. Based on the received measurement results, the mean value of the researched size was calculated [24–39].

In Figures 10–17, the method of the measurement of cylindrical elements, and of the rectangular ones, manufactured with the application of DMLS, on which it is possible to observe the model structure (such as detail surface and the quality of workmanship), is presented. The holes, as well as the rectangular objects (Figures 14–17), were measured three times in the center and at both ends of the measured element.

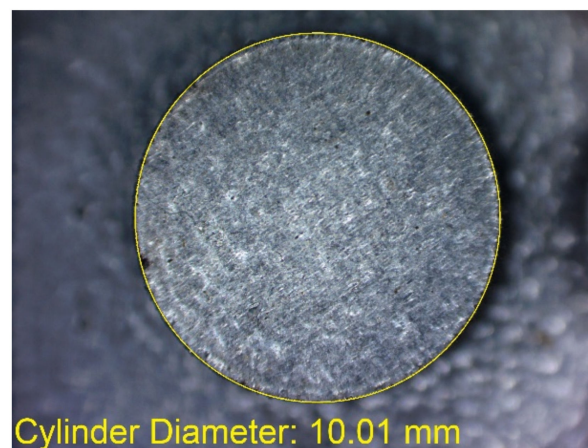


Figure 10. Measurement result for cylindrical holes and solids made in the DMLS technology: cylinder with a nominal diameter $D_d = \text{Ø}10$ mm ($D_{d1} = 10.01$ mm).



Figure 11. Measurement result for cylindrical holes and solids made in the DMLS technology: cylinder with a nominal diameter $D_m = \text{Ø}1$ mm ($D_{m1} = 0.99$ mm).

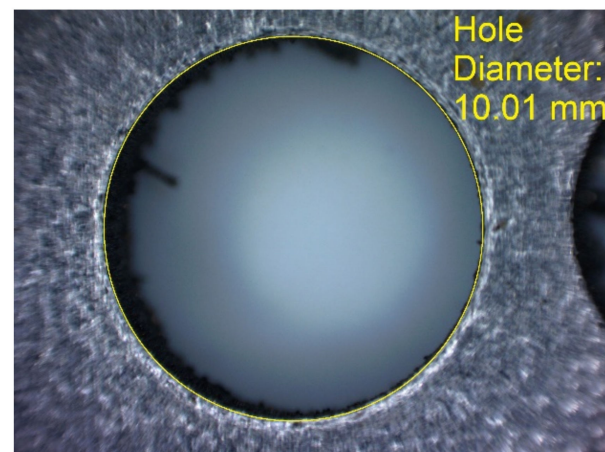


Figure 12. Measurement result for cylindrical holes and solids made in the DMLS technology: hole with a nominal diameter $D_d = \text{Ø}10$ mm ($D_{d1} = 10.01$ mm).

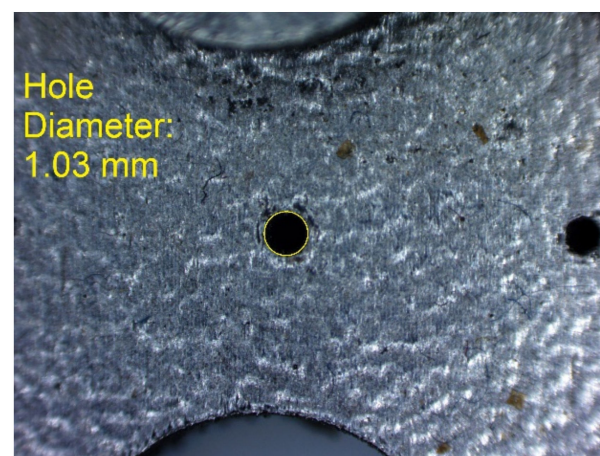


Figure 13. Measurement result for cylindrical holes and solids made in the DMLS technology: hole with a nominal diameter $D_m = \text{Ø}1$ mm ($D_{m1} = 1.03$ mm).

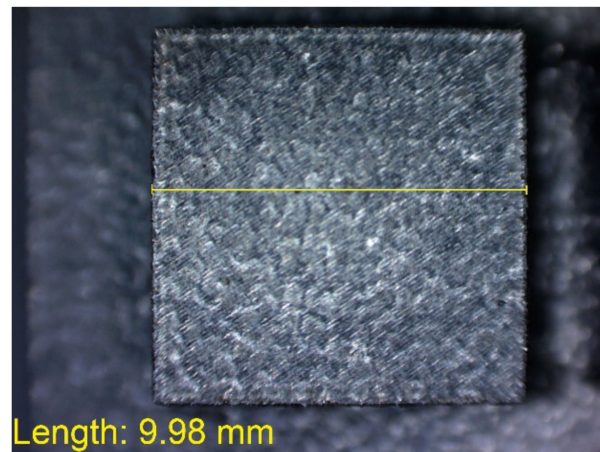


Figure 14. Measurement result for cuboidal holes and solids made in the DMLS technology: solid with a nominal width of 10 mm ($L_{dl} = 9.98$ mm).

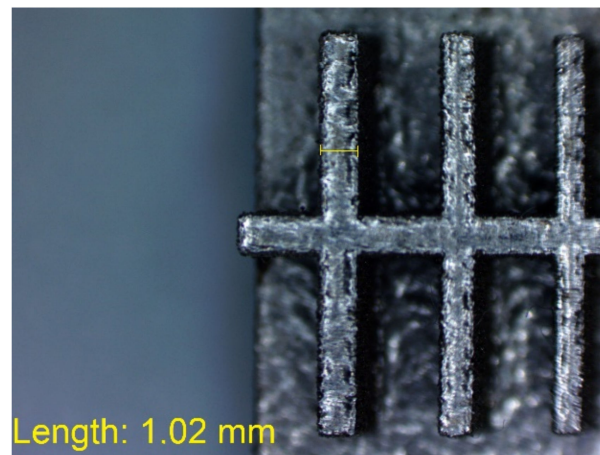


Figure 15. Measurement result for cuboidal holes and solids made in the DMLS technology: solid with a nominal width of 1 mm ($L_{m1} = 1.02$ mm).

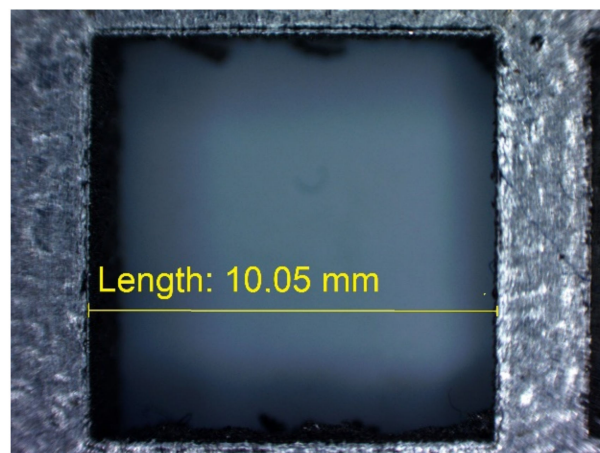


Figure 16. Measurement result for cuboidal holes and solids made in the DMLS technology: cuboidal hole with a nominal width of 10 mm ($L_{dl} = 10.05$ mm).

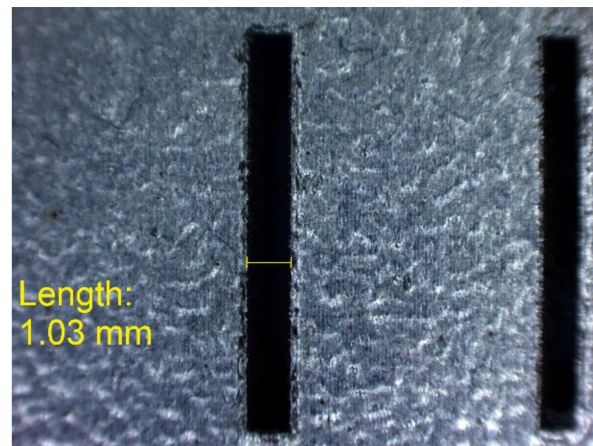


Figure 17. Measurement result for cuboidal holes and solids made in the DMLS technology: cuboidal hole with a nominal width of 1 mm ($L_{m1} = 1.03$ mm).

3. Results and Discussion

In Table 6, the received results relevant to manufactured prototypes measured with the application of an optical microscope, together with the calculated values of arithmetic means of the measured parameters, as well as deviations between the nominal dimension and the received mean values, are collated.

3.1. Comparison of the Obtained Results

The results received in the course of the research were divided into three parts. The first included those measurements that were divided in terms of the researched parameter, and the objective of that was to demonstrate differences between the nominal dimension (that assumed in the course of designing the details) and that received in the course of research.

In Figures 18–21, the received mean values of the result measurements relevant to cylindrical elements, and the names of the researched parameters that match the nominal dimension assumed in the course of designing research models, are presented.

Table 6. Measurement results of the research models made in DMLS technology from 17-4 PH stainless steel.

No.	Model	Measured Feature	Actual Value (B_1) [mm]	Measurement Results [mm]			Arithmetic Mean of the Measurement Results (B_2) [mm]	Difference between the Arithmetic Mean and the Actual Value ($B_2 - B_1$) [mm]
				1	2	3		
1	MB1	Hole Ø10 mm	10	10.01	10.01	10.01	10.01	0.01
		Hole Ø9 mm	9	8.98	9.00	8.98	≈8.99	−0.01
		Hole Ø8 mm	8	7.95	7.98	7.97	≈7.97	−0.03
		Hole Ø7 mm	7	6.95	6.95	6.95	6.95	−0.05
		Hole Ø6 mm	6	6.02	5.99	6.04	≈6.02	0.02
		Hole Ø5 mm	5	5.04	4.96	5.04	≈5.01	0.01
		Hole Ø4 mm	4	4.07	4.09	4.07	≈4.08	0.08
		Hole Ø3 mm	3	3.00	3.06	3.06	3.04	0.04
		Hole Ø2 mm	2	2.03	2.01	2.02	2.02	0.02
		Hole Ø1 mm	1	1.03	1.02	1.04	1.03	0.03
		Hole Ø0.9 mm	0.9	0.94	0.92	0.91	≈0.92	0.02
		Hole Ø0.8 mm	0.8	0.84	0.88	0.87	≈0.86	0.06
		Hole Ø0.7 mm	0.7	0.76	0.73	0.75	≈0.75	0.05
		Hole Ø0.6 mm	0.6	0.66	0.65	0.68	≈0.66	0.06
		Hole Ø0.5 mm	0.5	0.56	0.56	0.57	≈0.56	0.06
		Hole Ø0.4 mm	0.4	0.46	0.46	0.46	0.46	0.06
		Hole Ø0.3 mm	0.3	0.36	0.36	0.37	≈0.36	0.06
		Hole Ø0.2 mm	0.2	0.27	0.26	0.28	0.27	0.07
		Hole Ø0.1 mm	0.1	0.19	0.20	0.20	≈0.20	0.10
		2	MB2	Cylinder Ø10 mm	10	10.01	9.99	10.03
Cylinder Ø9 mm	9			8.96	8.99	8.99	8.98	−0.02
Cylinder Ø8 mm	8			7.96	7.97	7.96	≈7.96	−0.04
Cylinder Ø7 mm	7			6.95	6.97	6.98	≈6.97	−0.03
Cylinder Ø6 mm	6			5.98	5.95	5.97	≈5.97	−0.03
Cylinder Ø5 mm	5			4.98	4.97	4.97	≈4.97	−0.03
Cylinder Ø4 mm	4			4.00	4.01	3.99	4.00	0.00
Cylinder Ø3 mm	3			3.00	3.00	3.02	≈3.01	0.01
Cylinder Ø2 mm	2			2.01	2.02	2.00	2.01	0.01
Cylinder Ø1 mm	1			0.89	0.92	0.93	≈0.91	−0.09
Cylinder Ø0.9 mm	0.9			0.81	0.80	0.79	0.80	−0.10
Cylinder Ø0.8 mm	0.8			0.69	0.70	0.68	0.69	−0.11
Cylinder Ø0.7 mm	0.7			0.61	0.59	0.60	0.60	−0.10
Cylinder Ø0.6 mm	0.6			0.46	0.45	0.46	≈0.46	−0.14
Cylinder Ø0.5 mm	0.5	0.38	0.35	0.40	≈0.38	−0.12		
Cylinder Ø0.4 mm	0.4	0.26	0.25	0.26	≈0.26	−0.14		
		Cylinder Ø0.3 mm	0.3	cylinders impossible to measure				
		Cylinder Ø0.2 mm	0.2					
		Cylinder Ø0.1 mm	0.1					

Table 6. Cont.

No.	Model	Measured Feature	Actual Value (B_1) [mm]	Measurement Results [mm]			Arithmetic Mean of the Measurement Results (B_2) [mm]	Difference between the Arithmetic Mean and the Actual Value (B_2-B_1) [mm]
				1	2	3		
3	MB3	Hole width 10 mm	10	10.05	10.07	10.04	≈ 10.05	0.05
		Hole width 9 mm	9	9.04	9.04	9.06	≈ 9.05	0.05
		Hole width 8 mm	8	8.03	8.01	8.03	≈ 8.02	0.02
		Hole width 7 mm	7	7.01	7.01	7.03	≈ 7.02	0.02
		Hole width 6 mm	6	6.02	6.03	6.04	6.03	0.03
		Hole width 5 mm	5	5.06	5.06	5.06	5.06	0.06
		Hole width 4 mm	4	4.05	4.00	4.06	≈ 4.04	0.04
		Hole width 3 mm	3	3.00	2.98	3.01	≈ 3.00	0.00
		Hole width 2 mm	2	1.96	1.93	1.96	1.95	-0.05
		Hole width 1 mm	1	1.03	1.06	1.10	≈ 1.06	0.06
		Hole width 0.9 mm	0.9	0.96	0.98	0.96	≈ 0.97	0.07
		Hole width 0.8 mm	0.8	0.89	0.88	0.87	0.88	0.08
		Hole width 0.7 mm	0.7	0.75	0.78	0.77	≈ 0.77	0.07
		Hole width 0.6 mm	0.6	0.67	0.68	0.67	≈ 0.67	0.07
		Hole width 0.5 mm	0.5	0.58	0.58	0.58	0.58	0.08
		Hole width 0.4 mm	0.4	0.50	0.43	0.49	≈ 0.47	0.07
		Hole width 0.3 mm	0.3	0.38	0.39	0.35	≈ 0.37	0.07
		Hole width 0.2 mm	0.2	0.30	0.30	0.28	≈ 0.29	0.09
		Hole width 0.1 mm	0.1	0.22	0.19	0.20	≈ 0.20	0.10
				Solid width 10 mm	10	9.96	9.98	9.94
Solid width 9 mm	9			8.95	8.94	8.95	≈ 8.95	-0.05
Solid width 8 mm	8			7.95	7.93	7.97	7.95	-0.05
Solid width 7 mm	7			6.98	6.95	7.01	6.98	-0.02
Solid width 6 mm	6			5.99	5.99	6.02	6.00	0.00
Solid width 5 mm	5			5.00	5.00	5.00	5.00	0.00
Solid width 4 mm	4			4.00	4.00	3.99	≈ 4.00	0.00
Solid width 3 mm	3			3.01	3.03	3.01	≈ 3.02	0.02
Solid width 2 mm	2			2.00	2.01	2.02	2.01	0.01
4	MB4			Solid width 1 mm	1	1.02	0.98	0.98
		Solid width 0.9 mm	0.9	0.92	0.93	0.91	0.92	0.02
		Solid width 0.8 mm	0.8	0.81	0.82	0.80	0.81	0.01
		Solid width 0.7 mm	0.7	0.72	0.71	0.68	≈ 0.70	0.00
		Solid width 0.6 mm	0.6	0.59	0.62	0.64	≈ 0.62	0.02
		Solid width 0.5 mm	0.5	0.50	0.52	0.54	0.52	0.02
		Solid width 0.4 mm	0.4	0.38	0.44	0.44	0.42	0.02
		Solid width 0.3 mm	0.3	0.34	0.36	0.33	≈ 0.34	0.04
		Solid width 0.2 mm	0.2	0.20	0.20	0.20	0.20	0.00
		Solid width 0.1 mm	0.1	0.10	0.10	0.13	0.11	0.01

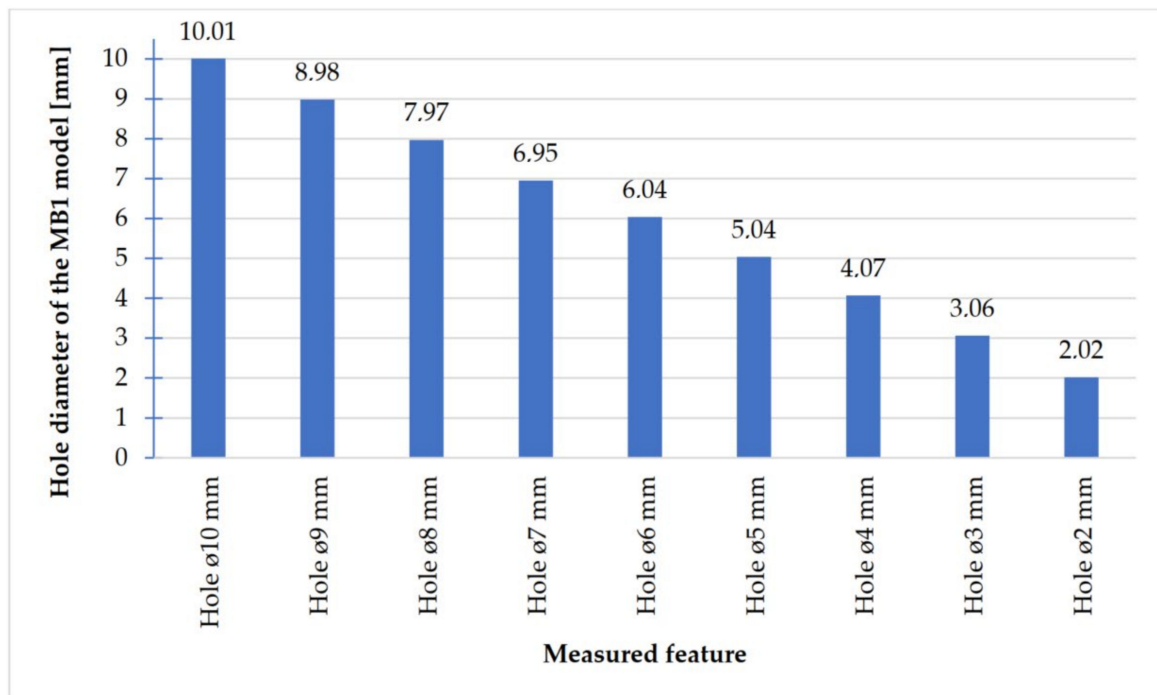


Figure 18. Average values calculated based on the cylindrical holes measurement results with dimensions \varnothing 10– \varnothing 0.2 mm.

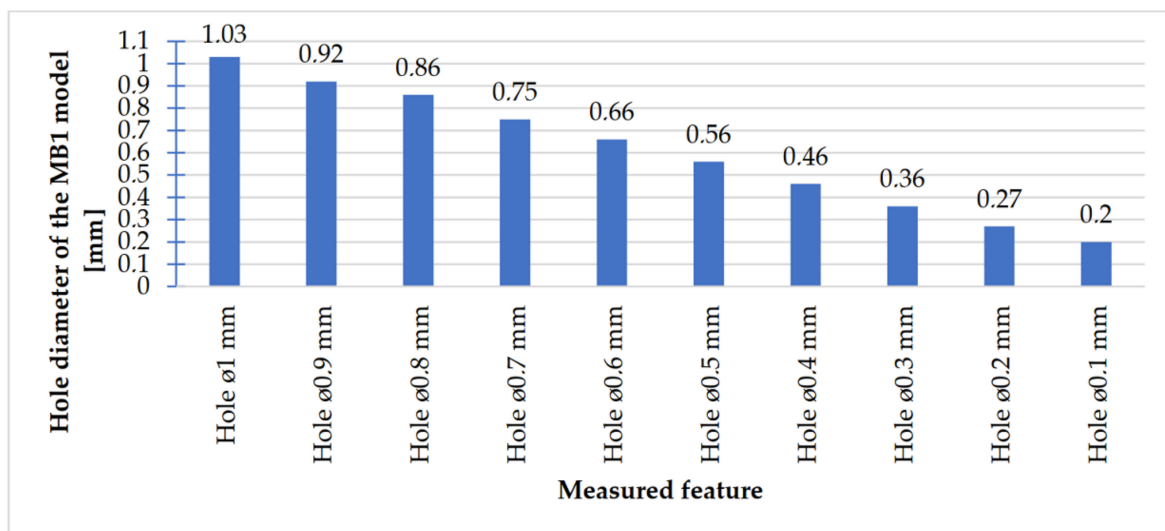


Figure 19. Average values calculated based on the cylindrical holes measurement results with dimensions \varnothing 1– \varnothing 0.1 mm.

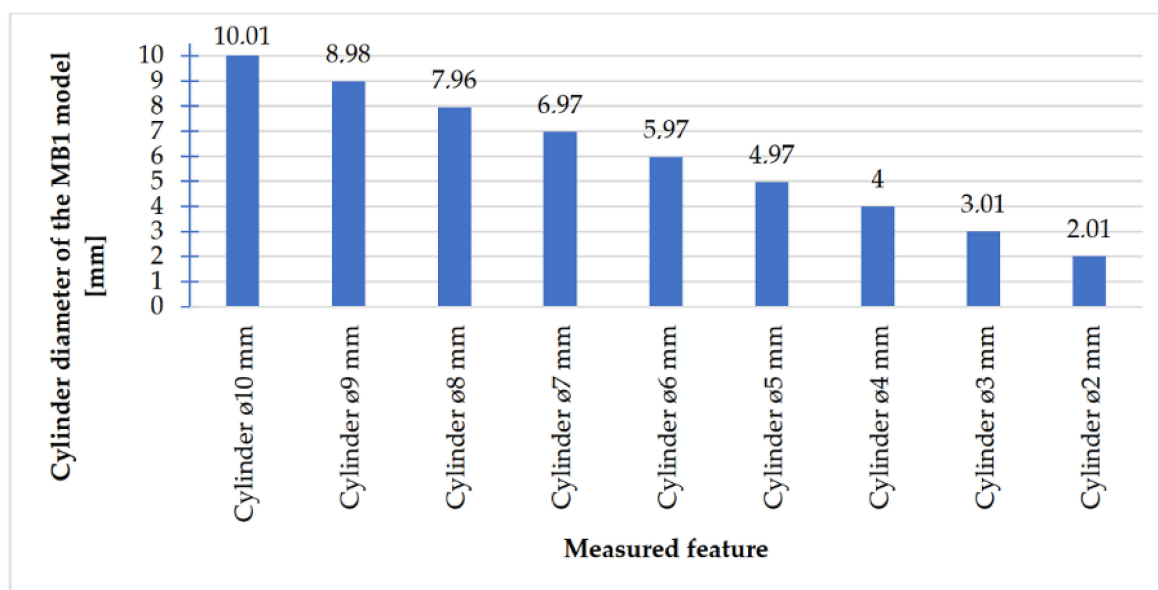


Figure 20. Average values calculated based on the cylinders measurement results with dimensions Ø10–Ø2 mm.

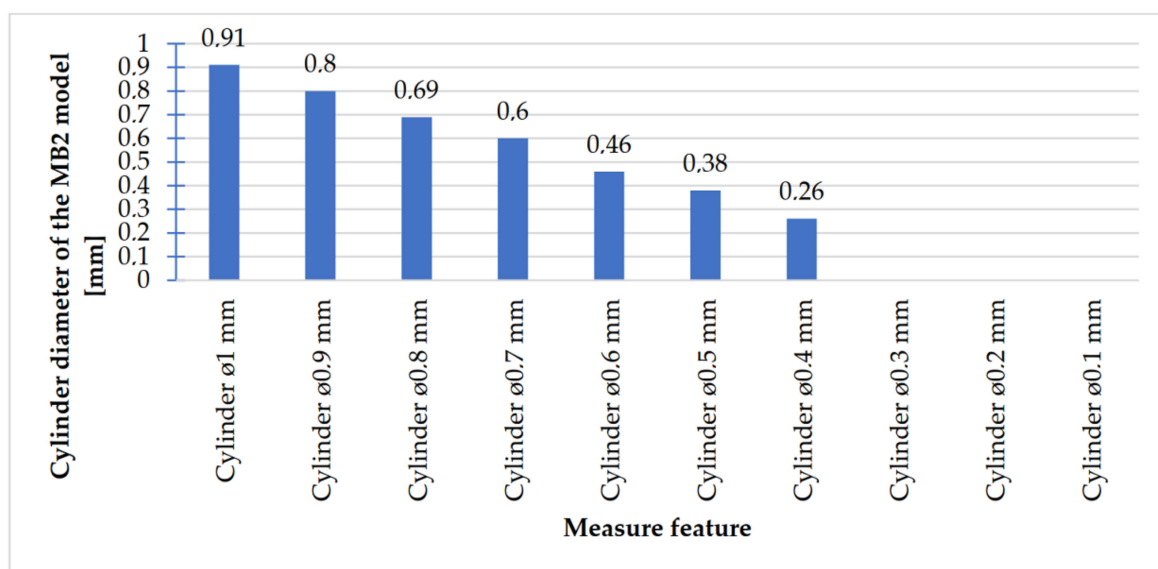


Figure 21. Average values calculated based on the cylinders measurement results with dimensions Ø1–Ø0.1 mm.

Comparing the values received in the course of the measurements of cylindrical holes with the dimension assumed in the course of designing details that are presented in Figure 6c,d, it is ascertained that they were comparable with the nominal dimensions of the researched parameters. All the holes within the considered range were manufactured in research details. The situation was the same in the case of cylinders (Figure 7a,b), where the measured values were also similar to the nominal dimension, wherein the following range of cylinders: Ø1–Ø0.1 mm, the accuracy of workmanship and reducing cylinder diameter was decreasing. It is also worth adding that all the cylinders having the assumed diameters were manufactured with the application of the analyzed DMLS; however, the height of the cylinders (namely, Ø0.3, Ø0.2, and Ø0.1 mm) was lower than those of the other ones, which resulted in it being impossible to calibrate a research device to fit their height, which is presented in Figure 22.

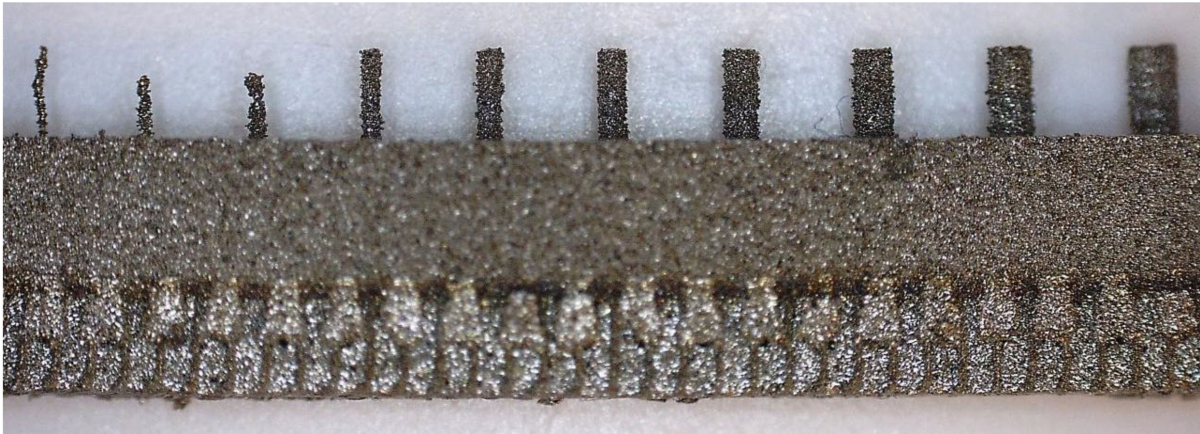


Figure 22. Front view of the model of cylinders with diameters of $\text{Ø}1\text{--}\text{Ø}0.1$ mm made of 17-4 PH steel.

In Figures 23–26, the received results of the measurements of cuboidal elements: holes, as well as objects in which the names of particular parameters match the assumed nominal dimension, are presented.

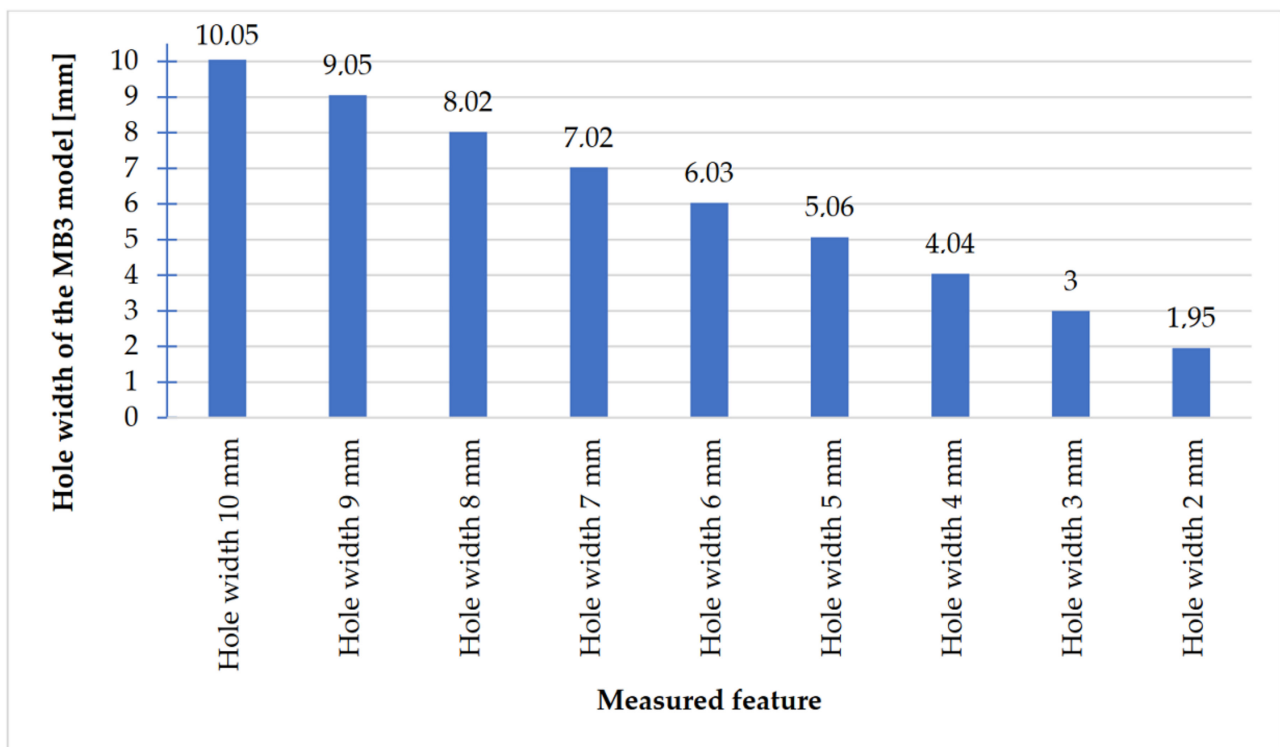


Figure 23. Values measured for rectangular holes 10 to 2 mm wide.

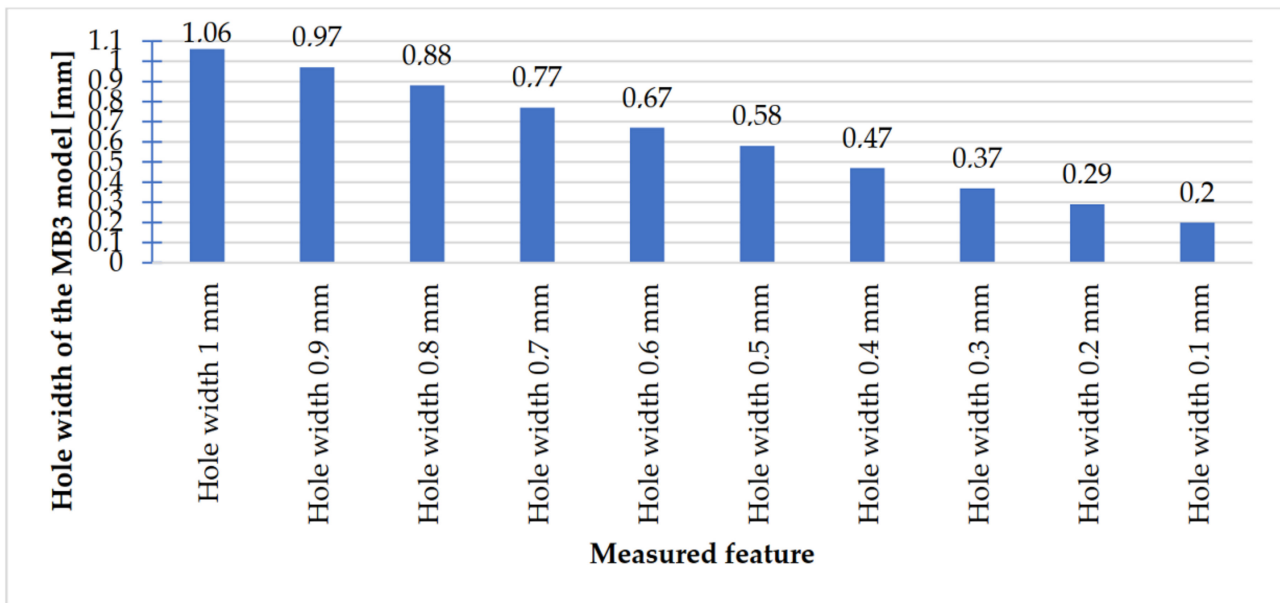


Figure 24. Measured values of rectangular holes in the range of 1–0.1 mm.

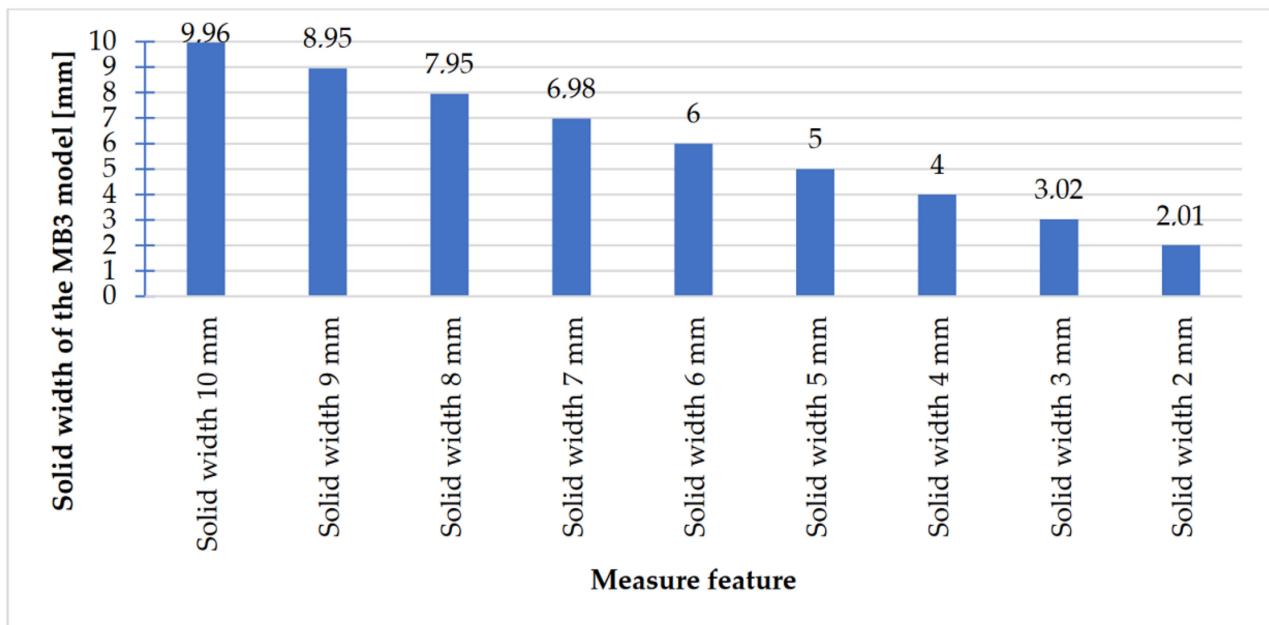


Figure 25. Measured values of rectangular solids with dimensions 10–2 mm.

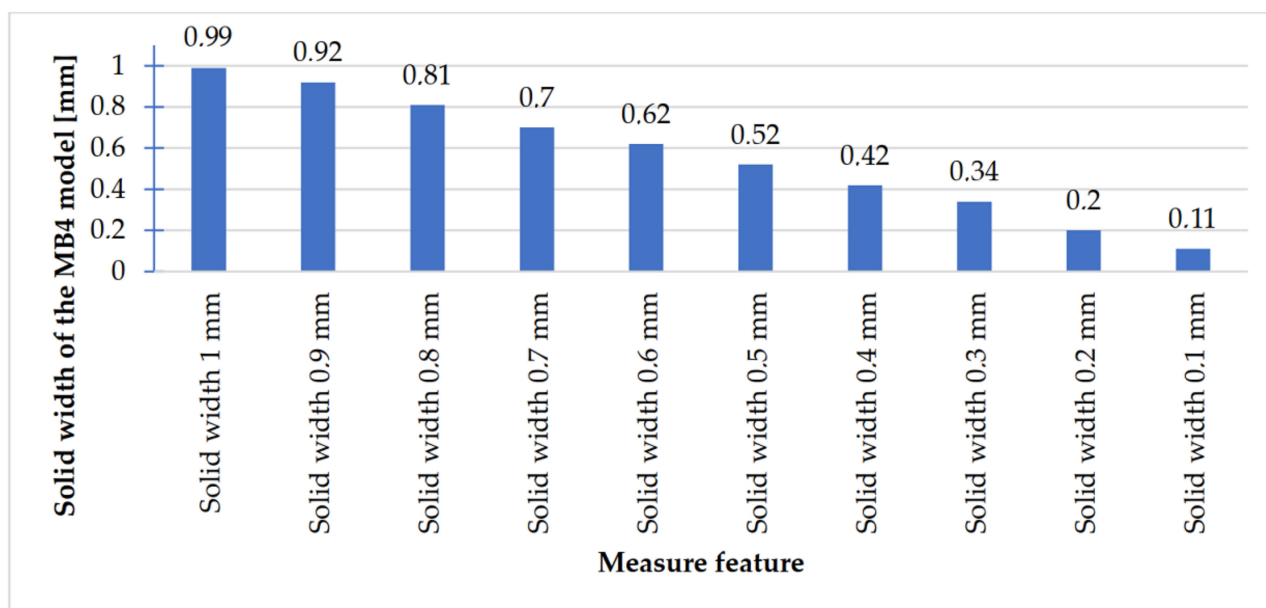


Figure 26. Measured values of rectangular solids with dimensions from 1 to 0.1 mm.

Comparing the values received in the course of the measurements of holes and rectangular objects, it is possible to observe that they are comparable with the nominal dimension for the researched parameter (Figures 8 and 9). It is also possible to observe that, for the holes having the following width: 0.1–1 mm (Figure 8c), results higher than the assumed sizes of the considered parameter were received. It is also worth mentioning that a nonsignificant deformation was observed only in the case of an object having a width of 0.1 mm, which is presented in Figure 27.



Figure 27. Presentation of the deformation of a fragment of a detail of a rectangular model made in the DMLS technology.

3.2. Comparison of the Difference between the Nominal and Measured Dimension

In the second part of the elaboration of the results of research into geometrical sizes, the values of deviations between the dimension assumed and that measured for the object models, as well as cylindrical and rectangular holes, were compared.

In Figures 28 and 29, the charts of deviations for rectangular models are presented.

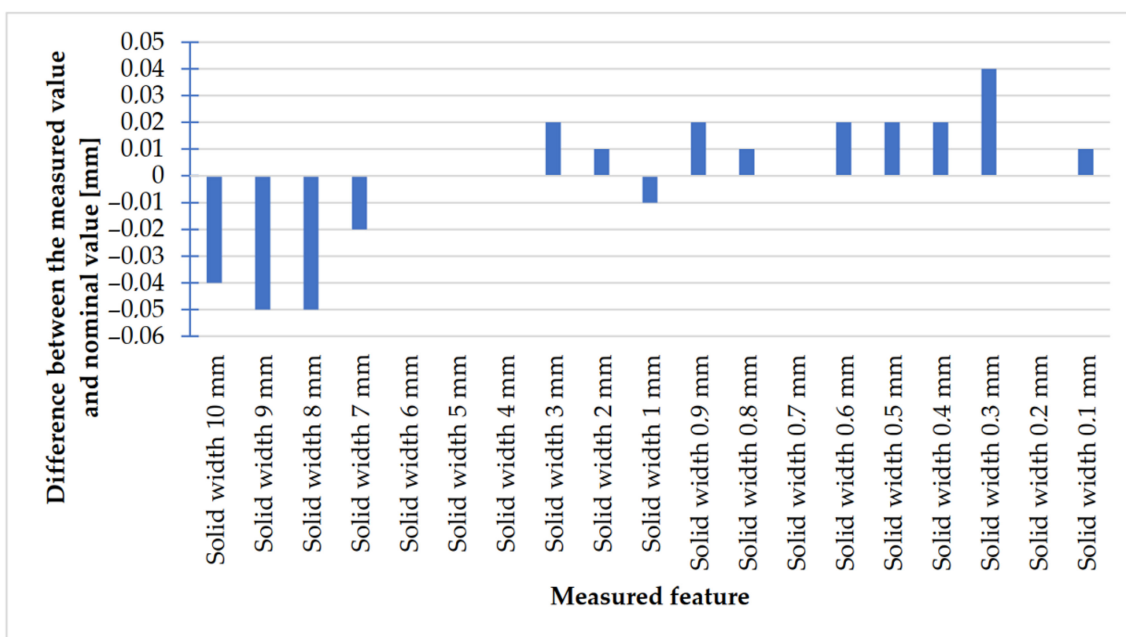


Figure 28. Deviation analysis for rectangular solids of variable width made in DMLS technology.

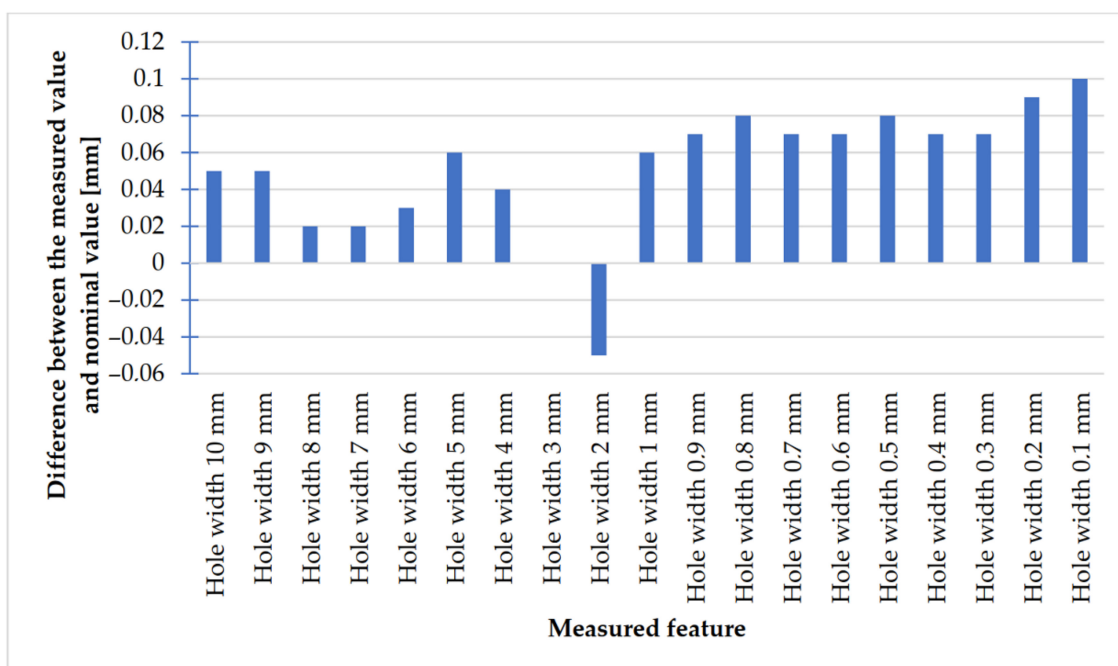


Figure 29. Deviation analysis for rectangular holes model made in the DMLS technology.

Looking at the chart presented in Figure 28, it is possible to observe that the values of deviations in the case of rectangular objects with the following widths: 10–7 mm were negative; in turn, the values of deviations in the case of objects with the following widths: 3–0.1 mm (except for an object with the width of 1 mm) were positive. The situation was the opposite in the case of rectangular holes (Figure 29), whose values of deviations were positive (except for holes with a width of 2 mm).

In Figures 30 and 31, the values of deviations in the case of cylindrical elements (holes and cylinders) are presented.

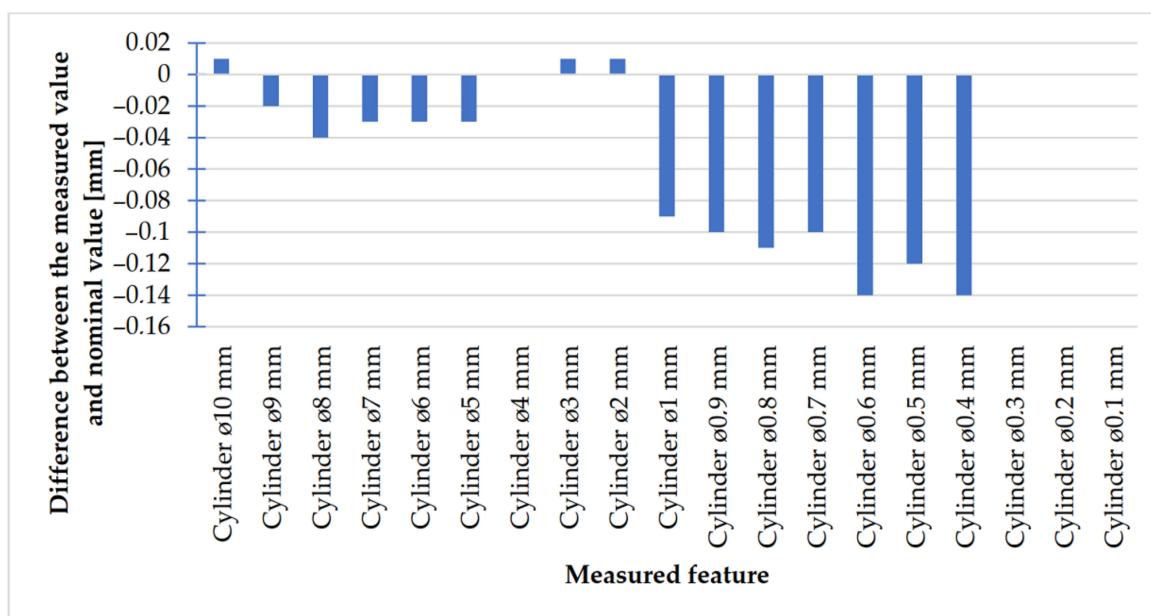


Figure 30. Deviation analysis for cylinders made in DMLS technology.

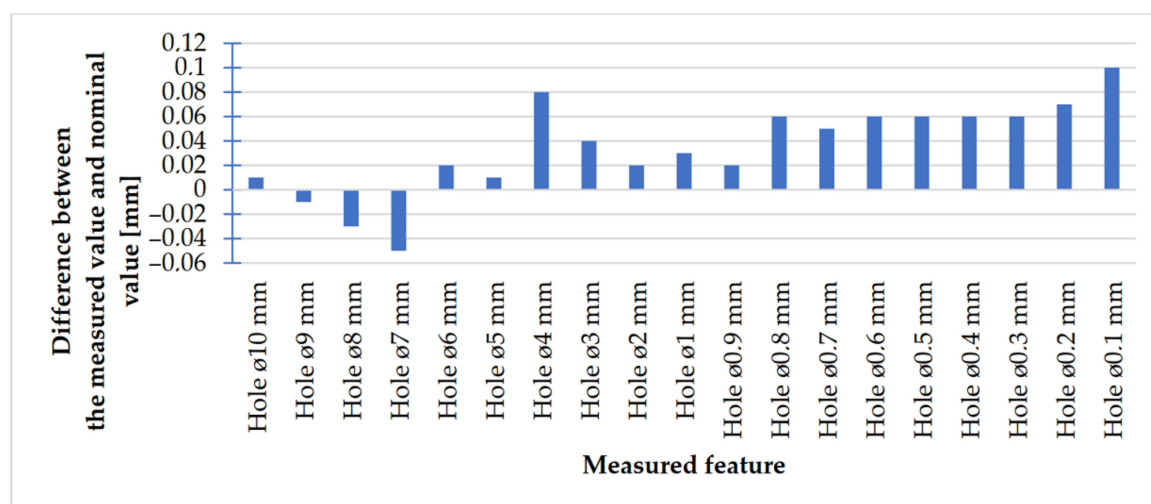


Figure 31. Deviation analysis for cylindrical holes with diameters from Ø10 to Ø0.1 mm of the model made in the DMLS technology.

In the cylinder model (Figure 30), in the course of the analysis of accuracy, it is possible to observe that, in the case of a cylinder with the dimension of Ø2 mm, the values of deviations were below 0.05 mm. In the case of cylinders with diameters of Ø1 mm and smaller, the values of deviations increased, unlike in the case of cylindrical holes (Figure 31), for which holes between Ø6 and Ø0.1 mm were associated with positive values within the following scope: 0.02–0.1 mm.

3.3. The Analysis of the Values of Means Deviations

In the third part of the elaboration of the measurement results, attention was focused upon the comparison of the largest and smallest absolute value, as well as the mean value of differences received as a result of research into rectangular and cylindrical models, and the mean values of deviations between the nominal dimension and that measured for spherical and angular models. The described collations are presented in Table 7.

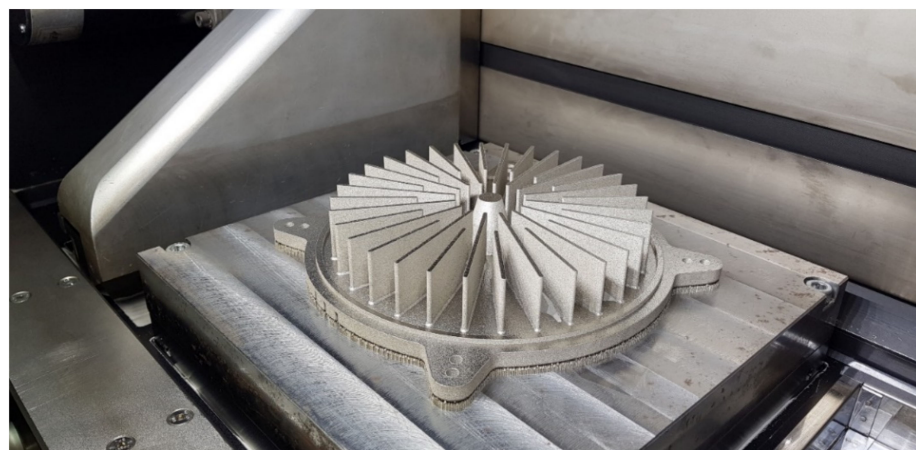
Table 7. Comparison of selected parameters of the research prototypes.

Research Prototype		Selected Parameters		
		The Largest Absolute Difference between the Nominal Dimension and the Measured *	Average Values of Deviations between the Nominal Dimension and the Measured	The Smallest Absolute Difference between the Nominal Dimension and Measured *
Cylindrical	Cylinders $\varnothing 0.1 \text{ mm} \div \varnothing 10 \text{ mm}$	0.14 mm ($\varnothing 0.6; \varnothing 0.4$)	0.04 mm	0 mm ($\varnothing 4$)
	Holes $\varnothing 0.1 \text{ mm} \div \varnothing 10 \text{ mm}$	0.10 mm ($\varnothing 0.1$)	0.03 mm	0.01 mm ($\varnothing 10; \varnothing 9; \varnothing 5$)
Rectangular	Rectangular holes width $0.1 \text{ mm} \div 10 \text{ mm}$	0.10 mm (0.1)	0.05 mm	0 mm (3)
	Rectangular solids width $0.1 \text{ mm} \div 10 \text{ mm}$	0.05 mm (8; 9)	0 mm	0 mm (6; 5; 4; 0.7; 0.2)

Comment: *—the parameters in parentheses refer to the feature that has reached the given dimension.

Based on the collation presented in Table 3, it is possible to observe that the greatest absolute difference between the nominal dimension and that measured in the case of cylindrical elements (both for the holes and objects) was ascertained in the case of cylinders within the following scope: $\varnothing 1\text{--}\varnothing 0.1 \text{ mm}$, contrary to the smallest absolute difference, which was observed in the case of elements within the following scope: $\varnothing 10\text{--}\varnothing 2 \text{ mm}$. In the case of the rectangular elements, it was impossible to observe such a correlation; however, in terms of rectangular holes, the greatest mean value of deviations between the nominal dimension and that measured for all the researched elements was observed.

In order to verify the received results, two radiators were referred to in the Introduction with appropriately shaped ribs with small cross-sections. In both of these cases, the ribs are arranged radially, which, in addition to anything else, may render manufacturing difficult (rake angle between a drift fender edge and a rib long edge ought not to be $0 [^\circ]$). In Figures 32 and 33, the radiators manufactured with the application of the DMLS methods are presented (variants 1 and 2) and designed in accordance with the assumptions determined at the beginning of this article, and also based on received research.

**Figure 32.** Radiator in the workspace of the EOS M270 variant No. 1.

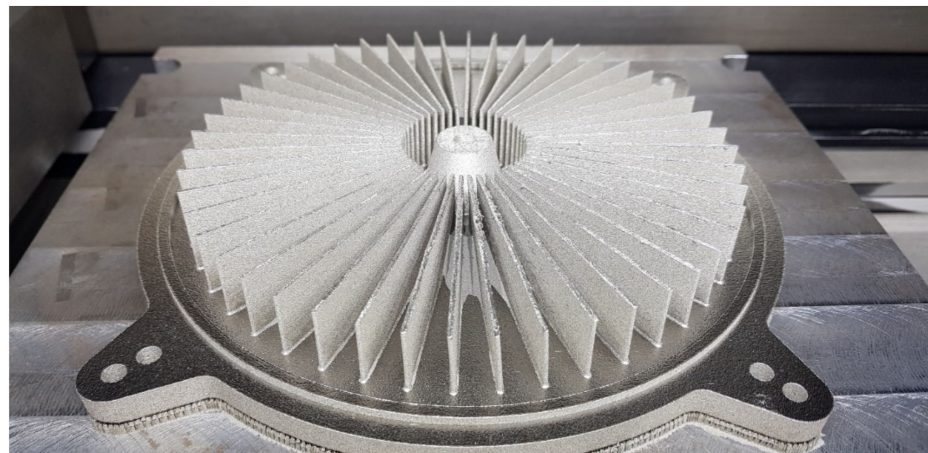


Figure 33. Radiator in the workspace of the EOS M270 variant No. 2.

4. Conclusions

The knowledge of the mechanical properties of materials renders it possible to design a given construction in a way that ensures that the loads caused in the course of operating it do not result in damage. It also refers to the ability of the material to be deformed in the course of being shaped. As observed based on the data contained in Table 1, the producer determined in detail and accurately the mechanical properties of the considered materials of which they had informed, which may prove that this material has been researched well. The resistance of the analyzed material is high (up to 1 GPa). The highest value for the 17-4 PH steel amounts to 40.8 HRC, which proves that the material is highly hard [40,41].

The research presented in the article was intended to show the possibility of manufacturing thin-walled structural elements that have a fulcrum only at the base. Additionally, already at the modeling stage of a complex structure, the constructor must have basic knowledge related to the specifics of the DMLS process. At this stage, the direction of the incremental forming in the DMLS method was determined, and it followed the direction of the material being applying by the recoater. Subsequently, the cross-section at the point of contact of the knife with the model should be as small as possible. It is related to the force exerted by the recoater on the model, which was minimal. Otherwise, the structure may deform or collapse, and thus, the process of forming the geometry will not process properly. Therefore, the article aimed to carry out research on the manufacture of thin-walled elements used in the construction of radiators. They were conditioned by the necessity to make radiators with an increased exchange surface through thin-walled elements such as ribs arranged in a radial manner. Manufacturing such long elements for a predetermined height in a radial manner can cause technological problems because it is impossible to arrange the research model in such a way that all the ribs are positioned in the direction of the thrust line of the recoater, which is consistent with the direction indicated by the red arrow (Figure 3).

The angle between the adjacent ribs of the radiator variant No. 2, which is presented in Figure 3, was almost zero. Thanks to the preliminary samples made with different wall thicknesses, it was possible to determine the minimum thickness of the rib and indicate the height so that the process was carried out correctly. The article presents two variants of radiator geometry (Figures 2 and 3) in order to confirm the validity of the research and the assumptions made. The article also takes a practical nature, indicating tendencies in the incremental formation of elements with small cross-sections. Thanks to the obtained results, it was also possible to determine whether the obtained geometries have an “on the plus” or “on the minus” tendency in relation to the nominal dimension determined during 3D-CAD geometry modelling. The obtained data were collected and presented in the form of graphs and tables. The experimentally determined research results for thin-walled models can be a kind of guide for the constructor during modelling geometries intended for additive

manufacturing. Furthermore, in this article, variants No. 1 and No. 2 of the radiator serve as examples of a functional prototype confirming the design assumptions that were determined after conducting a dimensional analysis of the MB1-MB4 research samples.

Based on the analysis of geometrical parameters contained in Table 4, it is possible to ascertain that the accuracy of the representation of prototype models is not much different from the 3D CAD model. The 17-4 PH steel is a material having high levels of mechanical properties, which is directly reflected in high-dimensional-shape accuracy of the manufactured details, in which, in the case of cylindrical and rectangular elements, deviations between the nominal dimension and that received in the course of the research were within the following scope: 0–0.1 mm.

The accuracy of manufacturing cuboidal and cylindrical research models was consistent with the parameters specified by the material manufacturer. The manufacturing of models in the range from $\varnothing 0.1$ to $\varnothing 0.3$ mm was problematic primarily for cylindrical models, as presented in Figure 22. However, for cuboidal models, the only deformations occurred in the model with a width of 0.1 mm, as presented in Figure 27. In the case of manufacturing holes in the research cylindrical models, their accuracy was much higher than in the case of cylindrical solids, which can be seen in Figures 18–21, Figure 30, and Figure 31. The value of the deviation between the nominal dimension and the average value obtained during measuring elements for rectangular holes in the width range from 10 to 0.1 mm was comparable and ranged from 0.02 to 0.1 mm, with two exceptions, which have been presented in Figure 29. Taking into consideration both cylindrical and cuboidal solids, elements in the range from 7 to 2 mm were characterized by the highest accuracy, which have been presented in Figures 28 and 29. Comparing the research models, cuboidal models were characterized by higher accuracy compared to the cylindrical models.

Comparing the photographs of the models taken in the course of the research stage, it was possible to ascertain that the staircase effect in the case of models manufactured with the application of DMLS was not observed and that the model structure was uniform.

Author Contributions: Conceptualization, G.B. and T.D.; methodology, G.B., T.D., Ł.P. and E.S.; software, G.B. and E.S.; validation, G.B. and Ł.P.; formal analysis, Ł.P.; investigation, Ł.P.; resources, M.D.; data curation, Ł.P. and M.G.; writing—original draft preparation, Ł.P.; writing—review and editing, Ł.P. and M.G.; visualization, Ł.P., M.D. and M.G.; supervision, G.B. and Ł.P.; project administration, G.B.; funding acquisition, G.B. and Ł.P. All authors have read and agreed to the published version of the manuscript.

Funding: This work was supported by the National Center for Research and Development, Poland. Grant No.: LIDER/6/0024/L-10/18/NCBR/2019.

Data Availability Statement: The data presented in this study are available on request from the corresponding author.

Conflicts of Interest: The authors declare no conflict of interest.

References

1. Gisario, A.; Kazarian, M.; Martina, F.; Mehrpouya, M. Metal additive manufacturing in the commercial aviation industry: A review. *J. Manuf. Syst.* **2019**, *53*, 124–149. [[CrossRef](#)]
2. Elakkad, A.S. 3D Technology in the Automotive Industry. *Int. J. Eng. Tech. Res.* **2019**, *8*, 248–251. [[CrossRef](#)]
3. Magerramova, L.; Vasilyev, B.; Kinzburskiy, V. Novel Designs of Turbine Blades for Additive Manufacturing. In Proceedings of the ASME Turbo Expo 2016: Turbine Technical Conference and Exposition, Seoul, Korea, 13–17 June 2016. [[CrossRef](#)]
4. Siemiński, P.; Budzik, G. *Additive Techniques. 3D Printing. 3D Printers [in Polish: Techniki Przyrostowe. Druk 3D. Drukarki 3D]*; Oficyna Wydawnicza PW: Warszawa, Poland, 2015; pp. 11–28.
5. Turek, P. Automating the process of designing and manufacturing polymeric models of anatomical structures of mandible with Industry 4.0 convention. *Polimery* **2019**, *64*, 522–529. [[CrossRef](#)]
6. Rokicki, P.; Budzik, G.; Kubiak, K.; Bernaczek, J.; Dziubek, T.; Magniszewski, M.; Nowotnik, A.; Sieniawski, J.; Matysiak, H.; Cygan, R.; et al. Rapid prototyping in manufacturing of core models of aircraft engine blades. *Aircr. Eng. Aerosp. Technol.* **2014**, *86*, 323–332. [[CrossRef](#)]

7. Rokicki, P.; Budzik, G.; Kubiak, K.; Dziubek, T.; Zaborniak, M.; Kozik, B.; Bernaczek, J.; Przeszlowski, L.; Nowotnik, A. The assessment of geometric accuracy of aircraft engine blades with the use of an optical coordinate scanner. *Aircr. Eng. Aerosp. Technol.* **2016**, *88*, 374–381. [CrossRef]
8. Dilberoglu, U.M.; Gharehpapagh, B.; Yaman, U.; Dolen, M. The Role of Additive Manufacturing in the Era of Industry 4.0. *Procedia Manuf.* **2017**, *11*, 545–554. [CrossRef]
9. Paszkiewicz, A.; Bolanowski, M.; Budzik, G.; Przeszlowski, L.; Oleksy, M. Process of Creating an Integrated Design and Manufacturing Environment as Part of the Structure of Industry 4.0. *Processes* **2020**, *8*, 1019. [CrossRef]
10. Rayna, T.; Striukova, L. From rapid prototyping to home fabrication: How 3D printing is changing business model innovation. *Technol. Forecast. Soc. Chang.* **2016**, *102*, 214–224. [CrossRef]
11. Anad, M.; Das, A.K. Issues in fabrication of 3D components through DMLS Technique: A review. *Opt. Laser Technol.* **2021**, *139*, 106914. [CrossRef]
12. PN/EN ISO/ASTM 52900:2017-06 Additive Manufacturing—General Principles—Terminology. Available online: <http://www.pkn.pl> (accessed on 11 December 2020).
13. Malladi, A.; Karunakaran, K. DMLS—An insight for unproblematic production. *Mater. Today Proc.* **2021**, *37*, 1986–1990. [CrossRef]
14. Lu, Y.; Badarinath, R.; Lehtihet, E.A.; De Meter, E.C.; Simpson, T.W. Experimental sampling of the Z-axis error and laser positioning error of an EOSINT M280 DMLS machine. *Addit. Manuf.* **2018**, *21*, 501–516. [CrossRef]
15. Wang, X.; Liu, Y.; Li, L.; Yenusah, C.O.; Xiao, Y.; Chen, L. Multi-scale phase-field modeling of layer-by-layer powder compact densification during solid-state direct metal laser sintering. *Mater. Des.* **2021**, *203*, 109615. [CrossRef]
16. Badiru, A.B.; Valencia, V.V.; Liu, D. *Additive Manufacturing Handbook: Product Development for the Defense Industry*; CRC Press: Boca Raton, FL, USA, 2017; pp. 162–164.
17. PN/EN ISO/ASTM 52901:2019-01 Additive Manufacturing—General Principles—Requirements Relevant to Parts Manufactured by Means of Additive Manufacturing (AM) Processes. Available online: <http://www.pkn.pl> (accessed on 18 December 2020).
18. PN/EN ISO 17296-2:2016-10 Additive Manufacturing—General Principles—Part 2: Overview of Process Categories and Feedstock. Available online: <http://www.pkn.pl> (accessed on 21 December 2020).
19. PN/EN ISO 17296-3:2016-10 Additive Manufacturing—General Principles—Part 3: Principal Characteristics and Appropriate Research Methods. Available online: <http://www.pkn.pl> (accessed on 21 December 2020).
20. PN/EN ISO 17296-4:2016-10 Additive Manufacturing—General Principles—Part 4: Overview of Data Processing. Available online: <http://www.pkn.pl> (accessed on 21 December 2020).
21. ISO/ASTM 52911-2:2019 Additive Manufacturing—Design—Part 2: Laser-Based Powder bed Fusion of Polymers. Available online: <http://www.pkn.pl> (accessed on 12 January 2021).
22. ISO/ASTM 52902:2019 Additive Manufacturing—Test Artifacts—Geometric Capability Assessment of Additive Manufacturing Systems. Available online: <http://www.pkn.pl> (accessed on 18 January 2021).
23. Kim, H.; Lin, Y.; Tseng, T.-L.B. A review on quality control in additive manufacturing. *Rapid Prototyp. J.* **2018**, *24*, 645–669. [CrossRef]
24. Moon, W.; Kim, S.; Lim, B.-S.; Park, Y.-S.; Kim, R.J.-Y.; Chung, S.H. Dimensional Accuracy Evaluation of Temporary Dental Restorations with Different 3D Printing Systems. *Materials* **2021**, *14*, 1487. [CrossRef] [PubMed]
25. Yoo, S.-Y.; Kim, S.-K.; Heo, S.-J.; Koak, J.-Y.; Kim, J.-G. Dimensional Accuracy of Dental Models for Three-Unit Prostheses Fabricated by Various 3D Printing Technologies. *Materials* **2021**, *14*, 1550. [CrossRef]
26. Msallem, B.; Sharma, N.; Cao, S.; Halbeisen, F.S.; Zeilhofer, H.-F.; Thieringer, F.M. Evaluation of the Dimensional Accuracy of 3D-Printed Anatomical Mandibular Models Using FFF, SLA, SLS, MJ, and BJ Printing Technology. *J. Clin. Med.* **2020**, *9*, 817. [CrossRef]
27. Dorweiler, B.; Baqué, P.E.; Chaban, R.; Ghazy, A.; Salem, O. Quality Control in 3D Printing: Accuracy Analysis of 3D-Printed Models of Patient-Specific Anatomy. *Materials* **2021**, *14*, 1021. [CrossRef]
28. Kačmarčík, J.; Spahic, D.; Varda, K.; Porca, E.; Zaimovic-Uzunovic, N. An investigation of geometrical accuracy of desktop 3D printers using CMM. *IOP Conf. Ser. Mater. Sci. Eng.* **2018**, *393*, 012085. [CrossRef]
29. Fahmy, A.R.; Becker, T.; Jekle, M. 3D printing and additive manufacturing of cereal-based materials: Quality analysis of starch-based systems using a camera-based morphological approach. *Innov. Food Sci. Emerg. Technol.* **2020**, *63*, 10238. [CrossRef]
30. Guo, B.; Xu, Z.; Luo, X.; Bai, J. A detailed evaluation of surface, thermal, and flammable properties of polyamide 12/glass beads composites fabricated by multi jet fusion. *Virtual Phys. Prototyp.* **2021**, 1–14. [CrossRef]
31. Kopsacheilis, C.; Charalampous, P.; Kostavelis, I.; Tzovaras, D. In Situ Visual Quality Control in 3D Printing. In Proceedings of the 15th International Joint Conference on Computer Vision, Imaging and Computer Graphics Theory and Applications, Valletta, Malta, 27–29 February 2020. [CrossRef]
32. Mitutoyo. Compendium of Metrology for Precision Measuring Instruments [In Polish: Kompendium Metrologii w Zakresie Precyzyjnych Przyrządów Pomiarowych]. Available online: https://www.mitutoyo.pl/application/files/1215/5888/6942/Mitutoyo_kompendium_metrologii_2013_WWW_opt_2.pdf (accessed on 30 March 2020).
33. Vagovský, J.; Buranský, I.; Görög, A. Evaluation of Measuring Capability of the Optical 3D Scanner. *Procedia Eng.* **2015**, *100*, 1198–1206. [CrossRef]
34. Dziubek, T.; Oleksy, M. Application of ATOS II optical system in the techniques of rapid prototyping of epoxy resin-based gear models. *Polimery* **2017**, *62*, 44–52. [CrossRef]

35. Siraj, I.; Singh Bharti, P. Reliability analysis of a 3D Printing process. *Procedia Comput. Sci.* **2020**, *173*, 191–200. [[CrossRef](#)]
36. Turek, P.; Budzik, G.; Sęp, J.; Oleksy, M.; Jóźwik, J.; Przeszłowski, Ł.; Paszkiewicz, A.; Kochmański, Ł.; Żelechowski, D. An Analysis of the Casting Polymer Mold Wear Manufactured Using PolyJet Method Based on the Measurement of the Surface Topography. *Polymers* **2020**, *12*, 3029. [[CrossRef](#)]
37. Paraskevoudis, K.; Karayannis, P.; Koumoulos, E.P. Real-Time 3D Printing Remote Defect Detection (Stringing) with Computer Vision and Artificial Intelligence. *Processes* **2020**, *8*, 1464. [[CrossRef](#)]
38. Octoprint. Available online: <http://www.octoprint.org> (accessed on 30 March 2020).
39. Matzkanin, G.A. Selecting a nondestructive testing method: Visual inspection. *AMMTIAC* **2006**, *1*, 7–10.
40. ISO/ASTM TR 52912:2020 Additive Manufacturing—Design—Functionally Graded Additive Manufacturing. Available online: <http://www.pkn.pl> (accessed on 5 January 2021).
41. ISO/ASTM 52911-1:2019 Additive Manufacturing—Design—Part 1: Laser-Based Powder Bed Fusion of Metals. Available online: <http://www.pkn.pl> (accessed on 12 January 2021).